

INVESTIGATING MORPHOLOGICAL STABILITY OF FACETED INTERFACES WITH AXIAL HEAT PROCESSING (AHP) TECHNIQUE

Reza Abbaschian*¹, Ercan Balikci¹, Andrew Deal¹, Michael Gonik², Viladimir D. Golyshev², Eddie Leonardi³, G. de Vahl Davis³, P.Y.P. Chen³, V. Timchenko³

University of Florida, Gainesville, FL, USA¹,
CTR “Thermo,” Alexandrov, Russia², University of New South Wales, Australia³

Abstract

Successful processing of homogeneous semiconductor single crystals from their melts depends strongly on precise control of thermal and fluid flow conditions near the solid/liquid interface. In this project, we utilize a novel crystal growth technique called Axial Heat Processing (AHP) that uses a baffle, positioned inside the melt near the interface, to supply and/or conduct heat axially to the interface. The baffle, which may or may not have a heater encased in it, can promote more stable and planar growth as well as reduce buoyancy driven convection. The latter is because the baffle reduces the aspect ratio of the melt as it separates the melt into three sections, above the baffle, in the feed gap between the baffle and the crucible wall, and below the baffle between the baffle base and the interface. AHP also enables a close monitoring and/or control of thermal boundaries near the solid/liquid interface during crystal growth by means of thermocouples placed in the baffle. The interface is kept planar when a heating element in the baffle is used. However, a proper choice of melt height is necessary to keep the interface planar when using the baffle without a heater. This study addresses the influence of melt height and growth velocity on the segregation profile of AHP-grown Sb doped Ge single crystals.

Introduction

Homogeneous single crystals of doped semiconductor materials are valuable to the electronic industry. The current Ultra Large-Scale Integration (ULSI) demands that the many wafers, cut from a melt-grown crystal, have consistently uniform electrical properties. This ensures a higher reproducibility and yield of solid-state devices. The solid/liquid (s/l) interface shape and convection in the melt mainly affect the homogeneity (e.g., solute segregation) in melt-grown crystals. A non-planar s/l interface can give rise to accumulation of the solute at depressed levels of the interface due to the gravity. Similarly, buoyancy driven or forced convection could cause fluctuations in the solute distribution at the interface. Since an uneven distribution of dopant results in the undesirable variation of electrical properties, several techniques have been utilized to eliminate segregation during crystal growth. These include the use of controlled thermal boundaries, magnetic fields, low gravity, and continuous feeding procedures¹⁻⁶. These methods focus on two principal factors to control segregation: the s/l interface shape and convection.

To achieve a homogeneous single crystal, it is clear that both convection and the s/l interface shape must be closely controlled. Current techniques to grow single crystals from the melt, such as the Czochralski, Float Zone, and Bridgman techniques, supply heat to the melt from radial sources. This leads to increased convection and non-planar interfaces¹. However, an alternate, novel processing technique called Axial

Keywords: characterization

* corresponding author email: rabba@mse.ufl.edu

Heat Processing (AHP) was developed in Russia to promote stable, planar crystal growth⁷. This technique has been used to grow single crystals with promising success⁸⁻¹². A comparable technique called the Submerged Heater Method (SHM) is currently under investigation by Ostrogorski et. al.¹³⁻¹⁵

AHP technique makes use of a baffle submerged in the melt near the s/l interface. The baffle may have a heater encased in it to supply heat axially to the growth interface. In the case when there is no heater in the baffle, the baffle may be made of a high conductivity material to still conduct the heat axially and distribute it over the growth interface. There are several advantages to having a baffle in the melt. First, the baffle minimizes the radial temperature differences created by the outside (background) heaters, promoting stable, planar growth. Second, the baffle separates the melt into two large regions. This effectively reduces the melt height above the interface, lowering the amount of buoyancy driven convection in that region. Third, by separating the melt into two regions, AHP can utilize the technique of Zone Leveling with starting charge only procedure^{14, 16, 17} to spread the dopant more evenly along the length of the crystal. Fourth, since the AHP method can promote planar growth and makes provisions to closely monitor the temperature of the growth domain, it is a suitable technique for studying interfacial kinetics and morphological stability.

The latter is the subject of current NASA supported international work exploring the fundamentals of faceted single crystal growth. This paper discusses the use of the AHP method to grow single crystals of Ge doped with Sb. AHP growth using a baffle with and without a heater is assessed. Influence of the melt height and growth velocity on the s/l interface shape, radial solute distribution, and morphological stability is analyzed. Some preliminary results have been already published elsewhere¹⁸⁻²⁰.

Experimental

Apparatus

Two different AHP units were used to grow Ge-Sb single crystals, one with a heater in the baffle and one without. Figure 1 shows a schematic of the AHP Unit-1. In this unit, the baffle (1) consists of a graphite shell encasing four C-type thermocouples and a Mo heating element (1-1). Two of the thermocouples record the temperature at the center of the baffle and the other two at the edges of the baffle near the crucible wall. All four are in the same plane, parallel to the base of the baffle. The crucible (2) is also made of graphite, and it has an internal diameter of 46 mm that holds the charge (C1 and C2) and a 20-mm thick disc-shaped seed (3). The charge may be placed in the crucible with two different compositions (C1 and C2), or it may be homogeneous. C₁ and C₂ regions are linked by a feed gap between the baffle and the crucible wall. The width of this channel is small enough (~ 0.5 mm) to prevent any back diffusion from the region below the baffle (C1) to the region above the baffle (C2)²¹. A cap (4) closes the crucible. The crucible is supported by a graphite pedestal (5) and a water-cooled Mo rod (6) that help extract heat from the growing crystal. During growth, the crucible is pulled down through a stationary, graphite guide tube (7). The guide tube is surrounded by a 4-zone background heater (furnace) (8), which provides heat to melt the charge and a portion of the seed. Additional thermocouples are located at strategic positions throughout the crucible, pedestal, and guide tube. A total of 19 thermocouples (T1-T19) monitor and/or control the thermal conditions in the unit. All of these components of the AHP unit are encased in a chamber, in which a vacuum/inert gas environment can be created.

Figure 2 shows a schematic of the AHP Unit-2. This unit also uses a graphite baffle (1) submerged in the melt near the solid/liquid (s/l) interface. However, no heater is placed in the baffle. The charge material is held in a 38.1-mm inner diameter graphite crucible (2), which again may have two different compositions

(C1 and C2) as explained above. A 20-mm high graphite insert (3) with a funnel shape cavity is also placed in the crucible to facilitate single crystal growth from a seed (4) of 5x5x17 mm prismatic shape. A cap (5) closes the crucible to prevent any loss of evaporates. A 3-zone radially heating vertical, tubular furnace (background heater) (6) supplies the required heat to melt the whole charge and a portion of the seed. Heat is extracted axially from the grown crystal through a graphite pedestal (7) and a Monel pedestal rod (8) by natural conduction (no water cooling). Ten calibrated K-type Inconel sheathed thermocouples (T1-T10) are positioned throughout the furnace, pedestal, crucible, and the baffle to control/monitor the thermal profiles. LabTech software controls the background heater zones with PIDs. A quartz retort (9), placed inside the background furnace, encases the aforementioned parts of the AHP unit and serves to create an inert gas atmosphere for the growth.

Procedures

In order to prevent evaporation of low melting point (630°C) Sb during heat up, a master charge of Ge-Sb alloy was prepared, which was then placed on the seed, and pure Ge chunks filled the crucible. The baffle was placed at the top of the solid charge. After positioning the crucible inside the furnace, the background heater was turned on to melt all of the charge and a portion of the seed. Next, the baffle was brought down until a desired initial melt height between the baffle and the seed is established. The baffle then was moved up and down a couple of times to stir the melt in order to create a homogeneous melt. Then, the growth was initiated by lowering the crucible, while the baffle and the background heaters (furnace) stayed stationary. The whole process took place under a slight argon overpressure. Experimental parameters of the crystals grown are given in Table I.

After growth, the samples were cut in half along their longitudinal axes and subsequently analyzed. One half of each sample was polished to a 1-micron finish using conventional metallographic techniques, and four-point probe resistivity measurements were taken to determine the Sb distribution in the samples. The resistivity measurements were done with a ~5 mm interval in radial and longitudinal directions, covering the entire surface of the half-cut sample. Finally, the samples were repolished to a 0.3-micron finish and etched with a 25:3:2 solution (by mass) of water, KOH, and $K_3[Fe(CN)_6]$ at 100°C for approximately 3 minutes to reveal microstructure, especially any possible growth striations.

Numerical Modeling

Crystal growth with the AHP Unit-1 was modeled using finite difference method in a two-dimensional cylindrical (r, z) coordinate system with the origin located at the bottom of the crucible (see Fig. 3). The movement of the incompressible viscous liquid in the melting zone was found by solving the Navier-Stokes equations with the Boussinesq approximation. The equations were written in a vorticity-Stokes stream function formulation. In the melt zone, both heat and solute transport were considered.

The solution of the transient solidification problem included explicit tracking of the solid/liquid interface. At each time step, the new location of the interface was determined. The Stefan condition as well as continuity at the interface was used for temperature, whilst a mass balance was used for the concentration. At the crucible walls, unsteady experimentally measured temperature values were imposed. At the axis of the cylinder (crystal), temperature and concentration fluxes were set to zero, as was the concentration flux at the free surface. At the other boundaries, continuity conditions for temperature and heat flux were imposed. Since a dilute alloy was considered, the melting temperature was taken as constant and equal to melting temperature of Ge.

The equations were non-dimensionalized using the following scaling factors: R_c , the crystal radius for length; $t_0 = R_c/u_0$ for time; $u_0 = v\sqrt{Gr}/R_c$ for the velocity and $\theta = (T - T_0)/\Delta T$ for temperature, where v is the viscosity, $\Delta T = T_{max} - T_0$, T_{max} is the maximum temperature in the melt and T_0 is the melting temperature of Ge.

The non-dimensional parameters Grashof (Gr), Prandtl (Pr), Schmidt (Sc), Stefan (St) and Peclet (Pe) numbers are defined as:

$$Gr = \beta_r g R_c^3 \Delta T / \nu^2, Pr = \nu / \chi_L, Sc = \nu / D_L, St = \gamma \rho_s / (\rho_L c_{pL} \Delta T), Pe = Pr \sqrt{Gr}, Pe_d = Sc \sqrt{Gr}$$

where β_r is the coefficient of volumetric expansion, g is the gravitational acceleration, χ_L is the thermal diffusivity of the melt, and D is the diffusion coefficient. Thermal conductivity λ , specific heat c_p , density ρ are non-dimensionalized by their value in the melt $\lambda_L, c_{pL}, \rho_L$,

$$\bar{\lambda} = \lambda / \lambda_L, \bar{c}_p = c_p / c_{pL}, \bar{\rho} = \rho / \rho_L.$$

In the region C_1 (see Fig. 3), the Navier-Stokes equations for an incompressible viscous liquid, in which the Boussinesq approximation is applied, may be written in vorticity-stream function form as:

$$\frac{\partial \omega}{\partial t} + D(\psi)\omega = \frac{1}{Re} \frac{1}{r} \left[\frac{\partial}{\partial r} \left(\frac{1}{r} \frac{\partial r^2 \omega}{\partial r} \right) + \frac{\partial}{\partial z} \left(\frac{1}{r} \frac{\partial r^2 \omega}{\partial z} \right) \right] + \frac{Gr}{Re^2} \frac{1}{r} \frac{\partial T}{\partial r}$$

and $\frac{1}{r} \left[\frac{\partial}{\partial r} \left(\frac{1}{r} \frac{\partial \psi}{\partial r} \right) + \frac{\partial}{\partial z} \left(\frac{1}{r} \frac{\partial \psi}{\partial z} \right) \right] + \omega = 0$ in which the stream function and vorticity are defined as

$$u = \frac{1}{r} \frac{\partial \psi}{\partial z}, w = \frac{1}{r} \frac{\partial \psi}{\partial r}, \text{ and } \omega = \frac{\zeta}{r} = \frac{1}{r} \left(\frac{\partial w}{\partial r} - \frac{\partial u}{\partial z} \right)$$

The equations for heat and mass transfer are solved in the region C_1

$$\frac{\partial T}{\partial t} + D(\psi)T = \frac{1}{Pe} \nabla^2 T, \quad \frac{\partial c}{\partial t} + D(\psi)c = \frac{1}{Pe_d} \nabla^2 c$$

In the above equations, the operator for the convective terms ($\phi = \omega, T, c$) is defined as

$$D(\psi)\phi = \frac{1}{r} \frac{\partial}{\partial r} \left(\frac{\partial \psi}{\partial z} \phi \right) - \frac{1}{r} \frac{\partial}{\partial z} \left(\frac{\partial \psi}{\partial r} \phi \right).$$

The equation for heat conduction is considered within the area occupied by the crystal and crucible walls:

$$\bar{c}_p \bar{\rho} \frac{\partial T}{\partial t} = \frac{1}{Pe} \nabla \cdot (\bar{\lambda} \nabla T)$$

Time dependent experimentally measured temperatures were imposed at the external boundary of the crucible, at the baffle heater and gap δ between the baffle heater and crucible wall. These transient values were recorded at the thermocouple locations; the temperature between these points was determined using interpolation techniques. The discontinuity of the properties λ, c_p and ρ and continuity of the heat flow are imposed at the crystal-crucible and melt-crucible boundaries:

$$[T] = 0, \quad \left[\frac{\bar{\lambda}}{Pe} \frac{\partial T}{\partial n} \right] = 0.$$

Here and below, $[]$ denotes the change of the function inside the brackets across the interface. A symmetry condition is imposed at the axis for both temperature and velocity. The normal component of the velocity

of the melt-solid interface, V_{n_z} , is determined at each time step from the Stefan condition

$$T = T_0, \quad \left[\frac{\bar{\lambda}}{Pe} \frac{\partial T}{\partial n_z} \right] + St V_{n_z} = 0,$$

where T_0 is the temperature at which phase change occurs. The vertical component of velocity at the inflow region (see Fig. 3) is determined from a mass balance, viz.:

$$V_{\delta} = -V \frac{R_h^2}{I - R_h^2}$$

where R_h is the radius of the baffle heater. The imposed stream function conditions on the top melt boundary therefore become:

$$\begin{aligned} \psi &= -V \frac{r^2}{2} \text{ for } 0 < r < R_h, \quad \frac{1}{r} \frac{\partial \psi}{\partial n} = 0 \text{ for } 0 < r < I, \\ \psi &= -V \frac{R_h^2}{2} + \frac{r^2 - R_h^2}{2} \frac{V R_h^2}{I - R_h^2} \text{ at } R_h < r < I \end{aligned}$$

On the phase change boundary and on the side surface of the melt: $\psi = 0, \quad \frac{1}{r} \frac{\partial \psi}{\partial n} = 0$

A symmetry condition for the concentration is imposed along the axis and a zero concentration flux set on the crucible wall and heater. The condition of the balance for the concentration flux and dependence of concentration in the solid and the liquid phases is determined by an equilibrium condition at the interface

$\frac{1}{Pe} \frac{\partial c}{\partial n_z} + V_{n_z} c = V_{n_z} c_s, \quad c_s - k_0 c$, in which k_0 is the partition coefficient. A mass balance condition is used

at the inflow region: $\frac{1}{Pe_d} \frac{\partial c}{\partial z} + (V - V_{\delta})c = (V - V_{\delta})c_2$

where c_2 is the concentration in Region C_2 . It is assumed that above the baffle heater, in C_2 (see Fig. 1), the melt is well mixed, and the concentration in this zone is time independent. The initial temperature distribution is set to $T(z) = T_0$ for the whole calculation domain. The initial melt velocity was set to zero.

Results

Sample Grown with the AHP Unit-1

Only one crystal was grown with the unit that used a graphite baffle with a heater encased in it. This crystal is designated as Sample I. Figure 4 shows the etched half of the crystal along with a schematic of its features, denoting the single and polycrystalline regions. The crystal was grown at 20 mm/h pulling rate. During the growth up to 25 mm, the crystal was melted back and regrown a couple of times by adjusting the temperature of the baffle to demarcate the s/l interface. Similar melt backs were also done towards the middle and end of the sample. Experimental temperature profiles show these thermal fluctuations, Figure 5. Numerical modeling predicted 0.3-0.4 cm/s flow velocity (indicating a well-mixed liquid) and change in the direction of streamlines due to the thermal oscillations, Figure 6. Although, the melt height below the baffle, h , changed in the range 5-20 mm during the melt backs, it stayed almost constant at ~ 20 mm during the growth (see Fig. 6). Clear striations appeared in the sample delineated the shape of the s/l interface at different times during growth. Convex, concave, and nearly planar interface shapes were observed during the growth depending on the change in the thermal profile around the interface. However, in all interface configurations, deviation from planarity was in the range 1.0-1.7 mm.

Radially averaged longitudinal, measured solute concentration data for Sample I is plotted in Figure 7a with different prediction methods to compare the experimental data with the theoretical predictions. The

upper boundary for solute build up in the AHP grown crystals is given by considering only diffusional mixing in a melt geometry similar to that in floating zone technique²². In contrast, the lower boundary is given by considering the complete mixing in the melt, again similar to floating zone melt geometry¹⁶. The equation describing these two different approaches is essentially the same with a different decay constant:

$$C_s = C_o [1 - (1-k)e^{-\lambda x}]$$

in which $\lambda = (kv/D)(1-e^{-(vh/D)})^{-1}$ for diffusional mixing in the melt and $\lambda = k/h$ for complete mixing in the melt, where C_s is the solute concentration in the solidified crystal, C_o is the initial solute concentration in the melt, k is the partitioning coefficient, v is the growth velocity, D is diffusion coefficient of solute in the melt, h is the melt height, x is the distance solidified, and λ is the decay constant. The plots in Figure 7 were constructed by using these two approaches with $k = 0.003$ and $D = 5 \times 10^{-5} \text{ cm}^2/\text{s}$. The plot in Figure 7a shows that appreciable mixing took place during the growth of Sample I as also predicted by the numerical model. Axial solute concentration data for this sample, obtained via numerical modeling, matched the experimental data fairly well, Figure 8. Radial solute segregation in this sample ranged from 10% to 50% and shown in Figure 9a. In general, whenever the interface was close to planar, the radial segregation was minimal. High radial segregation (50%) was observed during the thermal fluctuations mentioned earlier. Also, comparison of Figure 9 with Figure 4 shows that high points on radial concentration profiles coincide with the low points of the striations appeared in the sample.

Samples Grown with the AHP Unit-2

Four samples were grown with this unit that used a baffle without a heater and a conical insert to facilitate single crystal formation. Two of the four samples, grown at 3 mm/h (Sample II) and 5 mm/h (Sample III), were completely single crystal. The other two samples grown at 10 mm/h (Sample IV) and 20 mm/h (Sample V), on the other hand, displayed columnar growth after a single crystal region. In Sample III, the cellular growth appeared at 22 mm from the top of its conical portion as seen in Figure 10, as compared with only 6 mm in the sample grown at 20 mm/h velocity (Sample V). In both samples, outline of the interface breakdown region resembled the shape of the conical insert.

Axial dopant concentration of the crystals increased smoothly as seen in Figure 7b-e. However, radial solute segregation in the crystals changed depending on the melt height below the baffle and growth velocity, Figure 9b-e. At the beginning, the radial segregation was 20% in Sample II, grown at 3 mm/h. Later, the segregation further increased to about 30% for a short distance and then started decreasing down to 8% at the end of the growth. For this sample, the melt height was initially 9 mm and increased about 75% at the end. On the other hand, Sample III, grown with 5 mm/h velocity, showed about 1.5% radial segregation at the beginning, which progressively increased to 45% at the end of the growth as the melt height decreased 45% from its initial value of 13 mm. Sample IV, grown with 10 mm/h velocity, had 25% radial segregation at the beginning, and it increased to 75% before the interface breakdown occurred. The melt height increased about 15% from its initial value of 13 mm. Radial segregation was already 75% at the beginning of Sample V, grown at 20 mm/h rate. No further data collection was possible for this sample because the interface instability observed at 6 mm above its conical section as stated before. Melt height for this sample increased 50% from 12 mm during the growth.

Discussions

As already stated, the segregation in melt grown crystals is mainly controlled by the interface shape and convection, both of which can be modified by changing the experimental parameters. Reduction in melt height, which is one of the main features of the AHP method, decreases the buoyancy driven convection in molten solutions considerably. This in turn can decrease the radial segregation in growing crystals. The dimensionless Rayleigh (Ra) number describes the convection in molten solutions¹³.

$$Ra = \frac{g\beta G_L h^4}{\alpha v} \sim \frac{\text{buoyancy forces}}{\text{viscous forces}},$$

where g is the gravitational acceleration, β is the coefficient of thermal expansion for melt, G_L is the temperature gradient in the melt, h is the melt height, α is the thermal diffusivity, and v is the kinematic viscosity. For instance, in conventional crystal growth techniques, the initial melt height is usually in the order of 100 mm. However, the AHP technique reduces the melt height to around 10 mm, decreasing the Ra number of the melt by a factor of 10^4 . In our experiments, melt height was kept in the range 5-20 mm. It can be then deduced from the foregoing that in this study, buoyancy driven convection in the melt is lowered.

Although, the AHP method reduces the buoyancy driven convection significantly, it still creates a forced convection in the melt below the baffle by the flow of liquid from the region above the baffle to the region below the baffle (see Figure 1 for melt flow). The potency of the forced convection can be shown by defining a “characteristic ratio” as the ratio of the melt height below the baffle to the length of diffusion boundary layer in front of the growth interface. Length of the diffusion boundary layer is given as $2D/v$, where D is the solute diffusivity in the melt and v is the growth velocity^{23, 24}. Depending on the value of the characteristic ratio, forced convection can appreciably disturb the melt near the s/l interface. The disturbance will be less when the characteristic ratio is larger than 1 and vice versa.

Experimentally determined axial solute concentration data for Sample I, shown in Figure 7a, fall closer to the theoretical data obtained considering complete mixing in the melt. This unexpected observation could be a result of following reasons. The characteristic ratio for the growth of Sample I is in the range 2.77-11.11, indicating that forced convection was weak. However, the temperature fluctuations during the interface demarcations might have caused buoyancy driven convection that stirred the melt. Numerical model that used the experimental thermal data at the boundaries also predicted about 0.3-0.4 cm/s flow velocity, indicating a well mixed melt below the baffle. However, in spite of the convection (buoyancy and/or forced), the axial heat supplied by the heater in the baffle kept the s/l interface mostly planar, parallel to the base of the baffle. As seen in Figure 4, the deviation of the s/l interface from planarity is only 1.7 mm at the beginning and 1 mm later on. The planar interface also reflected itself in the plots of radial concentration data for Sample I, Figure 9a. In general, the radial segregation was about 10%, except for the 50% segregation observed at the beginning (14 mm from the seed base) where temperature fluctuations took place. Hence, so long as the interface is kept planar by axial heat supply, convection is not able to create radial segregation.

It was observed that the distance to interface breakdown depended on the initial solute concentration in the melt and the growth velocity, Table I. Two samples grown with 3 mm/h (Sample II) and 5 mm/h (Sample III) did not display any interface instability because apparently there was not enough solute build up at the interface to render the interface unstable due to their low growth velocity. On the other hand, the other

3 samples showed instability at different distances depending on their initial solute concentration and the growth velocity. The interface in Sample IV, grown at 10 mm/h velocity, became unstable after 22 mm. Sample V, grown at 20 mm/h rate, had the same initial solute concentration as in Sample IV; however, it went unstable only after 6 mm because of its higher growth velocity. In contrast, interface breakdown in Sample I, grown with 20 mm/h velocity using the AHP Unit-1 with a heater in the baffle, occurred at a longer length (72 mm) than that in Sample V, which was also grown with 20 mm/h velocity. This was partially because Sample I had a lower initial solute concentration, see Table I. Another reason for this observation may be the kinetic stability due to having a planar interface in Sample I.

Although Figure 7 indicates that all samples experienced a considerable amount of convection during growth, resemblance of the outline of the cellular region in Sample IV and Sample V to the shape of the conical insert can be evidence to the absence of complete mixing in the melt. If there had been a complete mixing, since the concentration everywhere in the melt would have been the same, shape of the interface breakdown would not have conformed to the shape of the insert.

It should be noted that the conical graphite insert is expected to significantly change the thermal profiles in the growing crystal. This is particularly significant for the present experiments, since the thermal conductivity of graphite is about 5 times larger than that of solid Ge. Thermal calculations will be conducted to incorporate the influence of the insert on the temperature fields and consequently the shape of the interface.

Conclusions

The AHP method uses an axial baffle with or without a heater in it. The baffle effectively reduces the melt height and consequently the buoyancy driven convection in the melt. However, the AHP method still creates a forced convection in the melt below the baffle. The experimental observations suggest that regardless of the growth velocity and perhaps the melt height, a planar growth interface can be achieved with the AHP method by use of a heating element in the baffle that is positioned near the s/l interface and supplies heat axially to it. This is because, in addition to supplying heat axially to the interface, the axial heater also homogeneously distributes the heat evenly over the growth interface. Thus, the baffle with heater forces the interface stay planar. On the contrary, a choice of proper melt height and efficient heat removal from the interface through the growing crystal seem to be important to keep the s/l interface planar during the growth from the melt by the AHP method without a heater in the baffle. By achieving a planar interface either way reduces the radial dopant segregation.

Acknowledgement

This work is supported by NASA under the grant # 450975812, entitled “Morphological Stability of Faceted Interfaces”. Also, M. Gonik and V. Golyshev acknowledge support from INTAS-ESA grant # 99-01814.

References

1. Muller, G. (Freyhardt, H. C., Managing Ed.). “Crystals 12: Growth, Properties, and Applications”, Springer Verlag, Berlin, Germany, 11-28 and 57-66 (1988).
2. Sen, S. and Wilcox, W. R. Influence of Crucible on Interface Shape, Position, and Sensitivity in the Vertical Bridgman-Stockbarger Technique. *Journal of Crystal Growth*, vol. 28, 36-40 (1975).
3. Tiller, W. A. Preferred Growth Direction of Metals. *Journal of Metals*, Transactions AIME, 847-855 (1957).

4. Koai, K., Sonnenberg, K., and Wenzl, H. Influence of Crucible Support and Radial Heating on the Interface Shape During Vertical Bridgman GaAs Growth. *Journal of Crystal Growth*, vol. 137, 59-63 (1994).
5. Meyer, S., Ostrogorsky, A. G. Interface Shape in the Bridgman Configuration with and without the Submerged Heater. *Journal of Crystal Growth*, vol. 166, 700-707 (1996).
6. Chang, C. E. and Wilcox, W. R. Control of Interface Shape in the Vertical Bridgman-Stockbarger Technique. *Journal of Crystal Growth*, vol. 21, 135-140 (1974).
7. Russian patent, #1800854. February 15, 1990.
8. Golyshev, V. D., and Gonik, M. A. A Temperature Field Investigation in Case of Crystal Growth from the Melt with a Plane Interface on Exact Determined Thermal Conditions. *Crystal Properties and Preparation*, vol. 36-38, 623-630 (1991).
9. Golyshev, V. D., Gonik, M. A., and Tsvetovskii, V.B. In Situ Measurement of Interface Supercooling during Growth of $\text{Bi}_4\text{Ge}_3\text{O}_{12}$ Single Crystals from the Melt. *Instruments and Experimental Techniques*, vol. 41, no. 5, 735-738 (1998).
10. Golyshev, V. D., Gonik, M. A., Tsvetovskii, V.B., Vasil'ev, Y.V., and Shlegel, V. N. In Situ Measurements of Melt Supercooling near the Solidification Interface in Crystal Growth of $\text{Bi}_4\text{Ge}_3\text{O}_{12}$. *Inorganic Materials*, vol. 35, no.6, 601-604 (1999).
11. Golyshev, V. D., Gonik, M. A., and Tsvetovskii, V.B. Problems of $\text{Bi}_4\text{Ge}_3\text{O}_{12}$ and $\text{Li}_2\text{B}_4\text{O}_7$ single crystal growth by crucibleless variant of AHP method. *Journal of Crystal Growth*, vol. 198-199, 501-506 (1999).
12. Golyshev, V. D., Gonik, M. A., Tsvetovskii, V.B., Vasil'ev, Y.V., and Shlegel, V. N. Determination of supercooling in the presence of macrosteps on the growing facet of BGO. *Journal of Crystal Growth*, vol. 216, 428-436 (2000).
13. Ostrogorsky, A. Diffusion-controlled distribution of solute in Sn-1%Bi specimens solidified by the submerged heater method. *Journal of Crystal Growth*, vol. 110, 950-954 (1991).
14. Ostrogorsky, A. and Muller, G. Normal and zone solidification using the submerged heater method. *Journal of Crystal Growth*, vol. 137, 64-71 (1994).
15. Marin, C. and Ostrogorsky, A. Growth of Ga-doped $\text{Ge}_{0.98}\text{Si}_{0.02}$ by Vertical Bridgman with a baffle. *Journal of Crystal Growth*, vol. 211, 378-383 (2000).
16. Pfann, W. G. "Zone Melting", John Wiley & Sons, NY, 199-214 (1966).
17. Bennett, D. C. and Sawyer, B. Single Crystals of Exceptional Perfection and Uniformity by Zone Leveling. *The Bell System Technical Journal*, vol. 35, 637-660 (1956).
18. Balikci, E., Deal, A., Abbaschian, R., Gonik, M.A., and Golyshev, V.D. "Growth of Antimony Doped Germanium Single Crystals by a Submerged Heating Technique." *Proceedings CD of the 2nd Pan Pacific Basin Workshop on Microgravity Sciences, Pasadena, California, (May 1 - 4, 2001)*.
19. Boykova, S.V., Golyshev, V.D., Gonik, M.A., Tsvetovsky, V.B., Abbaschian, R., and Balikci, E. "Influence of Varying Crystal Growth Conditions on the Behavior of Dopant Distribution for AHP Growth of Ge Crystals." *Proceedings of the Fourth International Conference, Single Crystal Growth and Heat & Mass Transfer, Obninsk, Russia, edited by V.P.Ginkin, vol. 4, 863-872 (Sept. 24-28, 2001)*.
20. Deal, A., Balikci, E., Abbaschian, R., Golyshev, V., Marchenko, M., and Leonardi, E. "Single Crystal Growth with Axial Heat Processing (AHP) Method." *Proceedings CD of the Conference on International Space Station Utilization, Kennedy Space Center, Florida (15-18 October 2001)*.
21. Golyshev, V. D., Gonik, M. A., and Csvetovsky, V. B. "Experimental Research of Longitudinal Segregation in growth by the AHP Method of Crystal Doped with Impurities with Small Value of the Distribution Coefficient." *Proceedings of the Joint Xth European and VIth Russian Symposium on Physical Sciences in Microgravity, St. Petersburg, Russia, vol. 2, 158-161 (15-21 June 1997)*.

22. Tiller, W. A., Jackson, K. A., Rutter, J. W., and Chalmers, B. The Redistribution of Solute Atoms During the Solidification of Metals. *Acta Metallurgica*, vol. 1, 428-437 (1953).
23. Burton, J. A., Prim, R. C., and Slichter, W. P. The Distribution of Solute in Crystal Grown from the Melt. Part I. Theoretical. *Journal of Chemical Physics*, vol. 21, no. 11, 1987-1996 (1953).
24. Fisher, K. "Fundamentals of Solidification." Trans Tech Publications, Switzerland, (1986).

Table I. Experimental parameters, cell incubation distance, and characteristic ratio.

Sample Number	C_o , ats. Sb/cc	v , mm/h	G_L , °C/cm	h , mm	Measured Cell incubation Distance, mm	$2D/v$, mm ($D=5 \times 10^{-5}$ cm^2/s)	Characteristic ratio = [$h/(2D/v)$]
I	5×10^{19}	20	10	5-20	72	1.8	2.77-11.11
II	5×10^{19}	3	17-10	9-16	No cells	12	0.75-1.33
III	1.10×10^{20}	5	6-7	13-7	No cells	7.2	1.8-0.97
IV	1.47×10^{20}	10	6-7	13-15	22	3.6	3.6-4.16
V	1.47×10^{20}	20	9-8	12-18	6	1.8	6.6-10

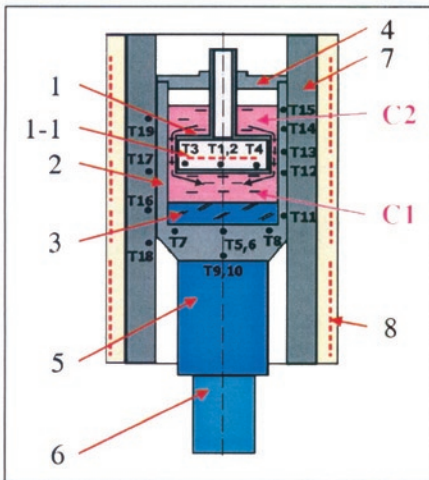


Figure 1. Schematic of the AHP Unit-1. The unit uses an axial baffle with a heater encased in it. Arrows around the baffle show the melt flow during the growth.

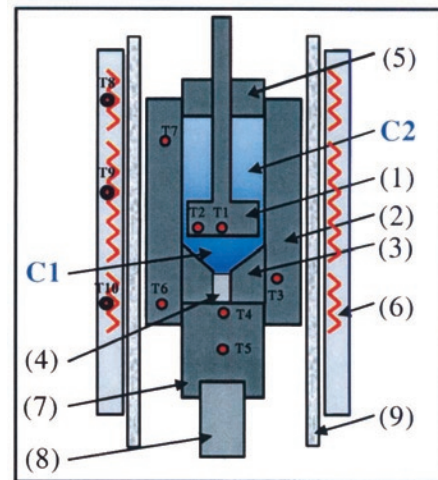


Figure 2. Schematic of the AHP Unit-2. The unit uses an axial baffle without a heater.

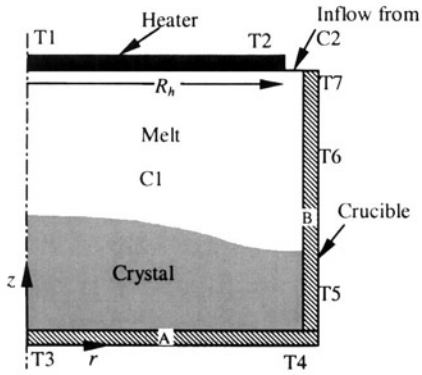


Figure 3. Computational domain.

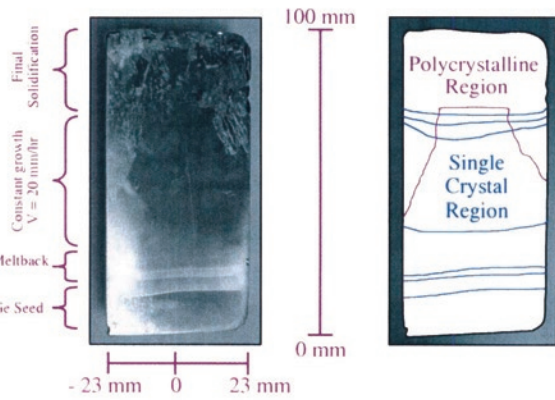


Figure 4. Sample I grown with the AHP Unit-1. Single, polycrystalline, and meltback regions are shown in the original photo and the schematic.

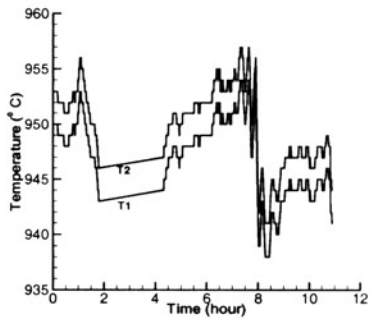


Figure 5. Thermal profile on the baffle (Thermocouples T1 and T2). Growth took place between 4.5th and 7th hours.

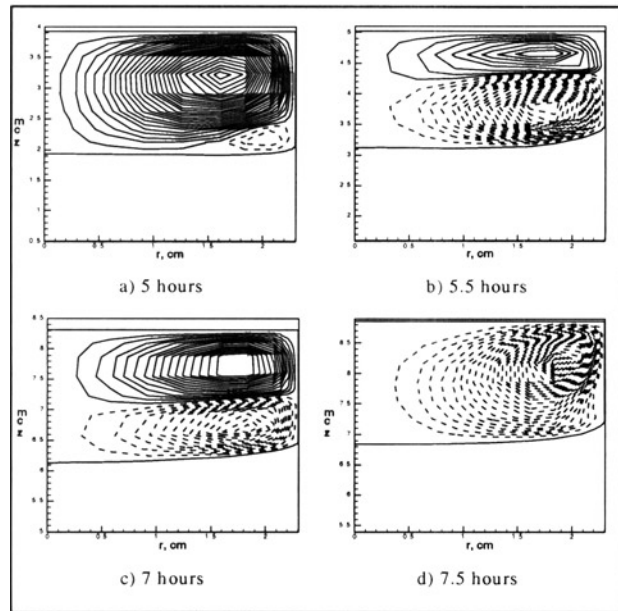


Figure 6. Stream functions during growth of Sample I. Dashed lines show the negative flow direction.

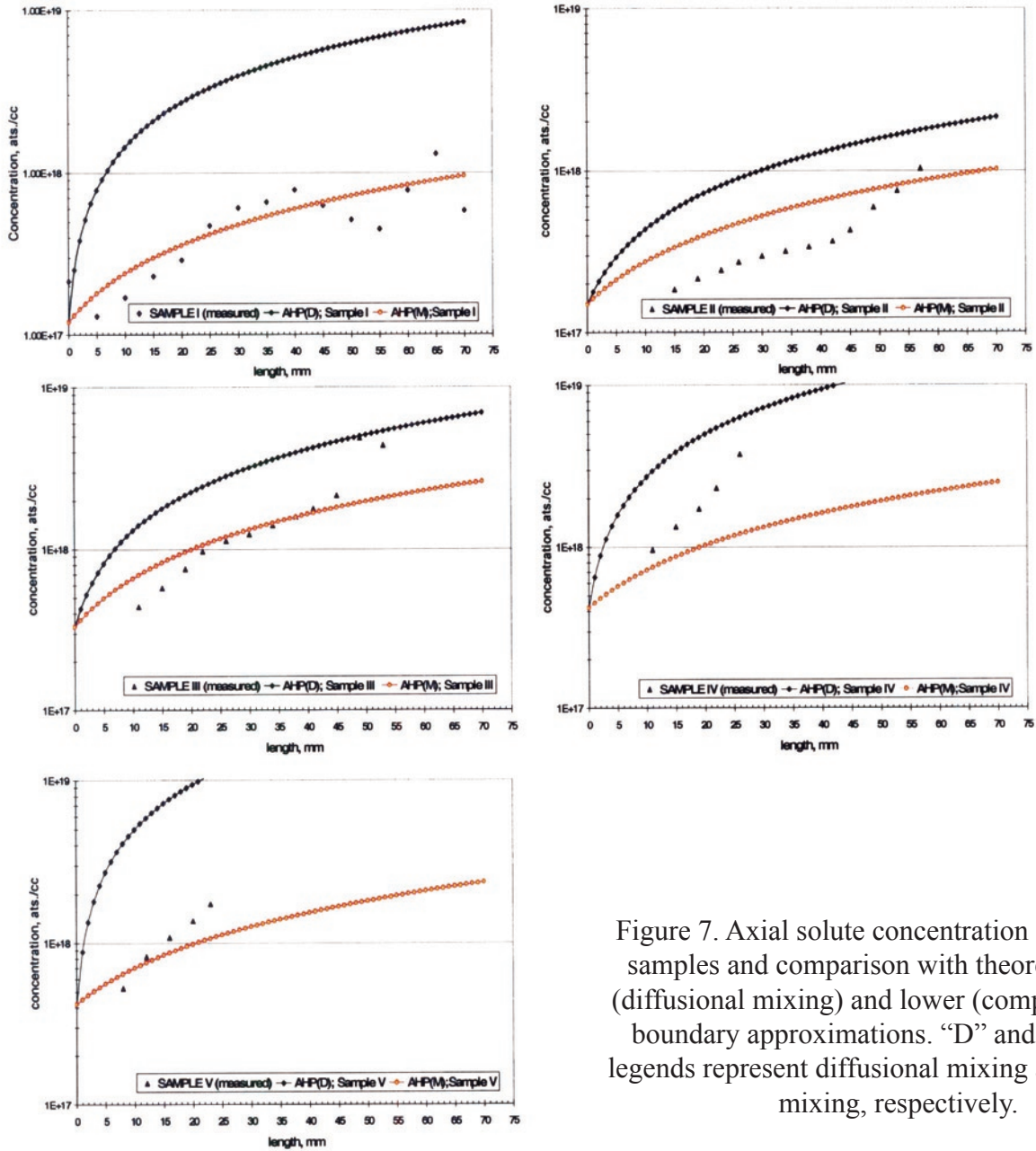


Figure 7. Axial solute concentration in the grown samples and comparison with theoretical upper (diffusional mixing) and lower (complete mixing) boundary approximations. “D” and “M” in the legends represent diffusional mixing and complete mixing, respectively.

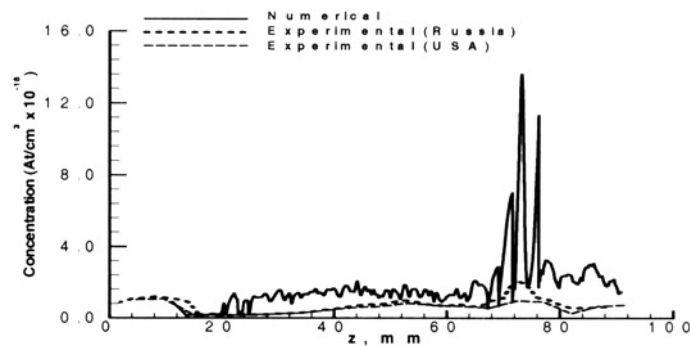


Figure 8. Axial solute distribution in Sample I, predicted by the 2-D numerical model and measured in two different laboratories in MSE-UF/USA and Russia.

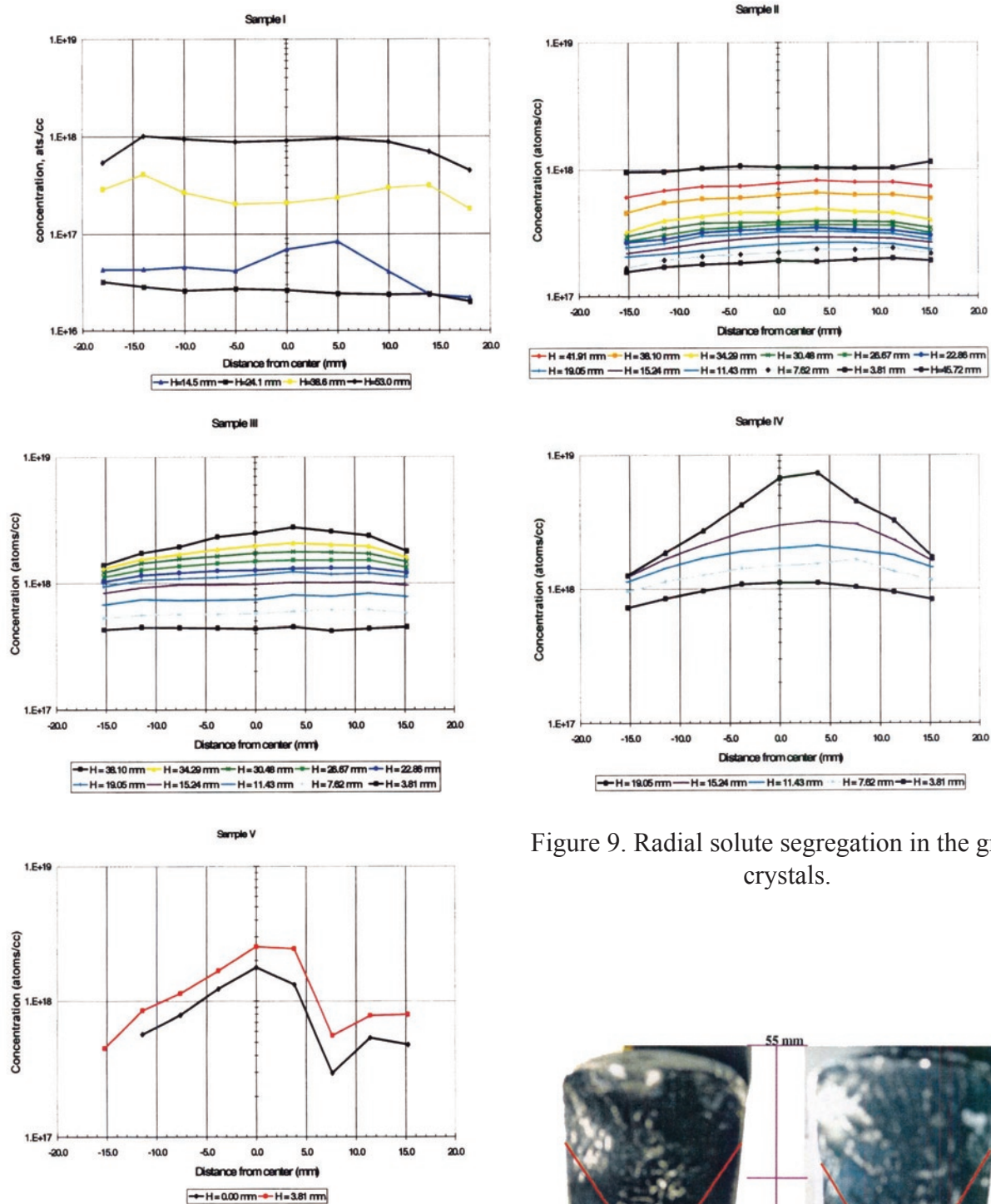


Figure 9. Radial solute segregation in the grown crystals.

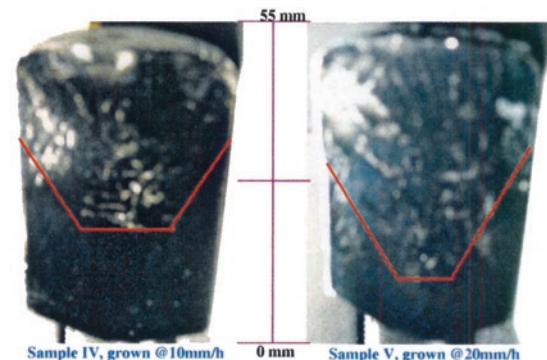


Figure 10. Interface breakdown in Sample IV and V. Outline of the breakdown resembles the shape of the conical insert.